The Egyptian Journal of Remote Sensing and Space Sciences 25 (2022) 961–974

HOSTED BY

Contents lists available at ScienceDirect

The Egyptian Journal of Remote Sensing and Space Sciences

journal homepage: www.sciencedirect.com

Research Paper

Past and future impacts of urbanisation on land surface temperature in Greater Cairo over a 45 year period

Sameh K. Abd-Elmabod [a,b,c,*], Marco A. Jiménez-González [d], Antonio Jordán [b], Zhenhua Zhang [e,f,*], Elsayed S. Mohamed [g], Amr A. Hammam [h], Ahmed A. El Baroudy [i], Mohamed K. Abdel-Fattah [j], Mahmoud A. Abdelfattah [k,l], Laurence Jones [m,n]

[a] Soils and Water Use Department, Agricultural and Biological Research Institute, National Research Centre, Cairo 12622, Egypt
[b] MED_Soil Research Group, Department of Crystallography, Mineralogy and Agricultural Chemistry, Seville University, Seville 41012, Spain
[c] Agriculture and Food Research Council, Academy of Scientific Research and Technology (ASRT), Cairo 11562, Egypt
[d] Geology and Geochemistry Department, Faculty of Sciences, Autonomous University of Madrid, Madrid 28049, Spain
[e] Jiangsu Key Laboratory for Bioresources of Saline Soils, School of Wetlands, Yancheng Teachers University, Yancheng 224007, China
[f] School of Agriculture and Environment, The University of Western Australia, Crawley, WA 6009, Australia
[g] National Authority for Remote Sensing and Space Sciences (NARSS), Cairo 11843, Egypt
[h] Department of Soils, Faculty of Agriculture, Minia University, Minia 61519, Egypt
[i] Soil and Water Department, Faculty of Agriculture, Tanta University, Tanta 31527, Egypt
[j] Soil Science Department, Faculty of Agriculture, Zagazig University, Zagazig 44519, Egypt
[k] Soils and Water Department, Faculty of Agriculture, Fayoum University, Fayoum 63514, Egypt
[l] Food and Agriculture Organization of the United Nations (FAO), Egypt
[m] UK Centre for Ecology & Hydrology, Environment Centre Wales, Deiniol Road, Bangor, Gwynedd LL57 2UW, UK
[n] Liverpool Hope University, Department of Geography and Environmental Science, Hope Park, Liverpool L16 9JD, UK

ARTICLE INFO

Article history:
Received 6 August 2022
Revised 3 October 2022
Accepted 4 October 2022
Available online 11 October 2022

Keywords:
Urban sprawl
LULC changes
Urban heat island (UHI)
Climate change
Nile Delta

ABSTRACT

Rapid and unplanned urbanisation can lead to altered local climate by increasing land surface temperature (LST), particularly in summer months. This study investigates the Urban Heat Island (UHI) in Greater Cairo, Egypt, using remote sensing techniques to estimate LST of summer months over 45 years (1986, 2000, 2017, and predicted year 2030). The research objectives and steps were, 1- mapped land use/ land cover (LULC), 2- conducted spatiotemporal analysis of LST, with a comparison of change in LST across different land cover types, 3- predicted future LST for 2030, and 4- examined this temporal change for a hot-spot area (ring road) and a cool-spot area (the River Nile). The results showed that urban areas have increased over the last 30 years by 179.9 km^2 (13 %), while agriculture areas decreased by 148 km^2 (12 %) and water bodies decreased by 6 km^2 (0.5 %). The mean LST over Greater Cairo increased over time, from 31.3 °C (1986) to 36.0 °C (2017) and is predicted to reach 37.9 °C in 2030. While a notable rise of mean LST in the Cairo ring road buffer zone (88 km^2), where it was 31.1 °C (1986), and 37 °C (2017) due to the triple increase of urban areas on account of agriculture areas, and the LST it may reach 38.9 °C by 2030. The mean LST increased slightly more in urban hot-spot areas than in cooler cultivated areas. UHI may induce a modification in the local climate that can negatively affect agricultural land, and human thermal comfort and unfortunately lead to a less sustainable environment.

1. Introduction

The population of the world is urbanizing rapidly. Over half of the world's population now lives in cities (McNabb, 2019), and this is projected to reach 68 % by 2050 (Ritchie & Roser, 2018). The rapid expansion of built-up areas can lead to wide-ranging environmental pressures worldwide (Yan et al., 2022). These effects include influences on food security, regional climate, hydrology and biodiversity (Huang et al 2020; Wang et al., 2022). The direct pressures that are produced by urbanisation tend to be localized around the cities themselves (Chen et al., 2022; Huang et al., 2022), and result from the conversion of surrounding land, which is very often agricultural land, to urban infrastructure. This results in a direct loss of the services that the agricultural land provided, including food production and carbon storage (Abd-Elmabod

* Corresponding authors at: Soil and Water Use Department, Agricultural and Biological Research Institute, National Research Centre, Cairo 12622, Egypt. Jiangsu Key Laboratory for Bioresources of Saline Soils, School of Wetlands, Yancheng Teachers University, Yancheng 224007, China.
E-mail addresses: sk.abd-elmabod@nrc.sci.eg (S.K. Abd-Elmabod), zhenhuaz70@hotmail.com (Z. Zhang).

https://doi.org/10.1016/j.ejrs.2022.10.001
1110-9823/

et al., 2019; Lin et al., 2021). It can also lead to degradation and a reduction in the ecological function of neighboring land due to proximity effects to cities, through impacts such as disturbance by people, noise pollution and reduced air quality (Huang et al., 2022). Another indirect local consequence can be on local climate, primarily through urban heat island effects where the temperatures of urban areas are higher than nearby rural temperatures (Zhao et al., 2007; Miao et al., 2022).

Urban Heat Island (UHI) effects occur by heat retention in constructed materials, and dissipated heat from domestic, commercial and industrial processes. UHI effects can also exacerbate urban air temperatures (Wang et al., 2022). Increased cooling demand for buildings transfers excess heat and humidity to the outside air leading to both increased heat and increased perception of heat in urban areas, which can threaten the health of inhabitants. Rapid urbanisation increases the extent and density of built-up areas (Du et al., 2017), and the loss of evapotranspiration cooling from vegetation, water bodies and natural areas further exacerbates the UHI (Alves et al., 2020). Vegetation cover has a direct effect on the local heat balance as the evapotranspiration process in plants absorbs the heat from the atmosphere to evaporate the water and shading directly reduces surface temperatures (Duveiller et al., 2018). So far, two main research methods have been used for studying UHI effects: meteorological observation and remote sensing data (Chudnovsky et al., 2004; Jin et al., 2011). Measurement of air temperatures using meteorological observation stations are typically located primarily in rural areas to avoid confounding effects such as those of the urban heat island. Geographically dispersed meteorological stations make spatial extrapolation difficult, especially in highly heterogenous areas like cities (Zhou et al., 2022). By contrast, satellite data provides high spatial resolution information on temperature, but at the moment is largely constrained to measurements of land surface temperature (Ali and Shalaby 2012; Chen et al., 2022; Gao et al., 2022). Thermal remote sensing imagery represents a vital tool to identify urban hotspots, cool spots and UHI intensity in order to propose heat mitigation strategies and enhance urban vegetation cover (Xian et al., 2022). Nonetheless, these can be highly valuable in ascertaining the relative influence of UHI effects, fine detailed pattern in UHI and particularly for monitoring changes in the extent of the UHI over time (Du et al., 2016; Du et al., 2017). Various researchers were used the Landsat images (TM, ETM + and OLI) to investigate LST and UHI phenomenon without immediate validation and depending on the previous validations of land satellite images that were presented in previous studies, and other researchers were focused in the validation process (Göttsche et al., 2013; Duan et al., 2021; Awais et al., 2022).

UHI effects have not been much studied in desert areas. Greater Cairo is a mega-city, with a population of 20 million, one of the largest cities in the Middle East and in Africa (Goussous & Tayoun, 2020). The urban area in the Nile Delta has increased dramatically in the last 30 years (Abd-Elmabod et al., 2019), and particularly around Greater Cairo. The increase of urban growth and infrastructure in Greater Cairo led to a loss of 7.7 % vegetation cover and an additional conversion of 8.7 % bare sand area to urban in the period 1990–2016 (Aboelnour & Engel, 2018). Over the same period, the urban microclimate has changed relative to agricultural areas (Aboelnour & Engel, 2018). LST increased over Greater Cairo during 2002 to 2012 and was 0.5 and 3.5 °C higher than average rural temperatures. These changes have been related to land use/ land cover, where the urban growth in the high density population areas as Greater Cairo showed the greatest increase in thermal radiation from land surfaces (Abutaleb et al., 2015). Recent studies (Athukorala and Murayama 2021) have shown differences in LST along an Urban–rural gradient, between the day and night, and the spatial characteristics of nighttime surface urban heat island effects over Greater Cairo. However, the long-term changes of LST have not been studied, and relatively little attention has been given to specific urban land covers that exacerbate heating or provide cooling. In addition, there have been very few projections of LST into the future.

Therefore, the current study aims to investigate relationships between land use/ land cover (LULC) and LST over time (1986, 2000 and 2017), and use these relationships to estimate future LST for the year 2030, in total spanning a 45 year period. The study focuses on calculating LST during the hottest summer months in locations within Greater Cairo and the surrounding Nile Delta region. Within the study, we document and project trends in LST temperature of Greater Cairo and its surroundings, and use specific examples to illustrate change in both hot spots of urban heat island using the Cairo ring road as a case study, and cool island (CI) spots of LST using the river Nile as a case study. Specifically, we address the following scientific questions:

How has LST changed over three decades, and how is it projected to change into the future based on current trends? What is the spatial pattern of LST change? Does the change rate of LST differ between UHI hotspots (built up areas and roads) and CI coolspots (cultivated and water bodies)?

2. Methodology

2.1. Study area (Greater Cairo)

The study area of Greater Cairo, Egypt is located at latitudes 29^{O} 45′ N – 30^{O} 16′ N and longitude 30^{O} 58′ E – 31^{O} 25′ E (Fig. 1), and it represents the 6th largest metropolitan area in the world and the largest urban area in Africa, the Arab world and the Middle east (Forstall et al., 2004). Three governorates (Cairo, Giza, and Qalyubia) are included in Greater Cairo, and the study area comprises the southern part of Nile delta and the northern part of Nile valley. The studied area extends west of Cairo, east of Giza, and south of Qalyubia with a total area of 1234 km^2 (Fig. 1), excluding newly cultivated land and urban areas on bare and marginal lands to the east and west. According to Cairo meteorological station data, the climate of greater Cairo is extremely arid where the annual precipitation < 20 mm /year, the average annual temperature is 22.2 ^{O}C, the maximum temperature of summer months 36.4 ^{O}C, and based on Köppen-Geiger climate classification the climate in Cairo was classified as a hot desert climate (BWh).

2.2. Satellite images and land use / land cover (LULC) classification

We used multi-temporal Landsat Thematic Mapper (TM) 1986, Enhanced Thematic Mapper Plus (ETM +) 2000, and Landsat-8 Operational Land Imager and Thermal Infrared Sensor (Landsat-8 OLI/TIRS) 2017 satellite imagery. Today, the USGS Landsat distribution scheme (https://www.usgs.gov/landsat-missions) allows the user to choose between a preprocessed dataset and a raw dataset. In this study, we used preprocessed datasets, downloaded from https://earthexplorer.usgs.gov/. Table 1 shows the features of the Landsat TM, ETM + and OLI satellite images used, while **Table S1** shows the descriptions of the satellite images used. In the preprocessed datasets we used, the digital number (DN) values of the multispectral bands, except for Band 9 in Landsat-8, have been converted into surface reflectance values, while those of the thermal bands have been converted into top of atmosphere brightness temperature expressed in Kelvin (USGS, 2016). The satellite images were masked to the study area and processed using ArcGIS 10.4 (ESRI, 2016).

LULC types of each year (1986, 2000, 2017) were classified separately using supervised classification (maximum likelihood)

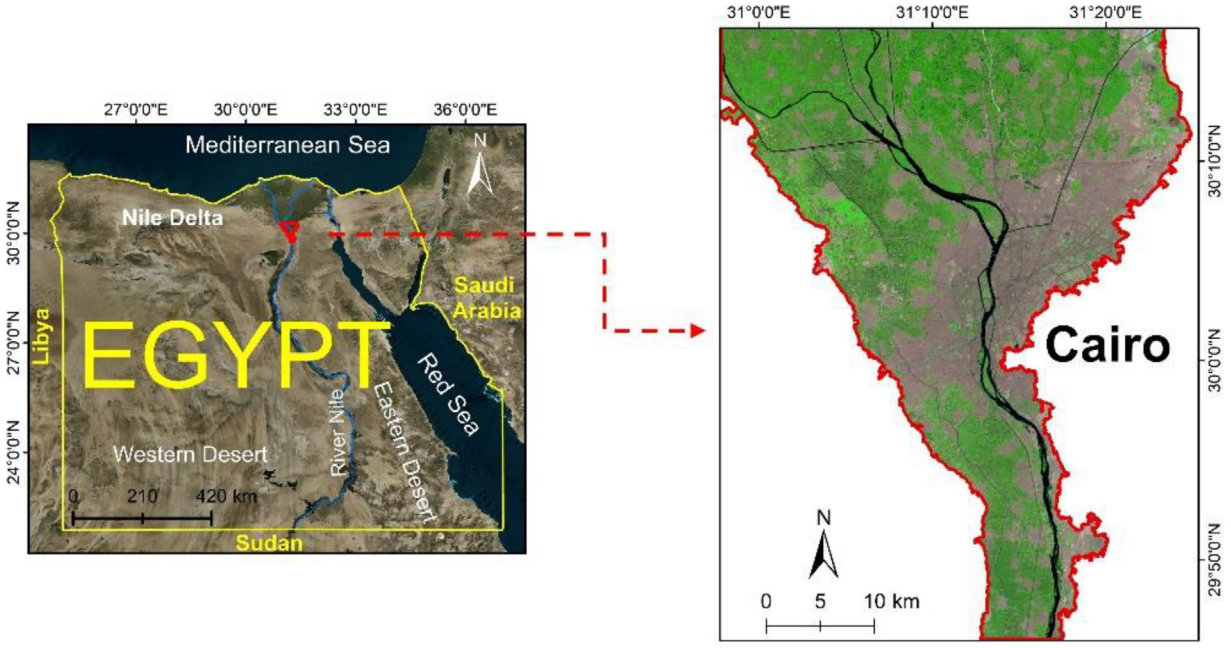

Fig. 1. Map of the study area, showing location of Egypt (left) and Greater Cairo (right).

Table 1
Features of the used Landsat TM, ETM + and OLI satellite images. NIR, Near Infrared; SWIR, Shortwave Infrared; TIR, Thermal infrared.

Landsat 5 TM			Landsat 7 ETM+			Landsat 8 OLI		
Band	**Spatial resol. (m)**	**Wavelength (μm)**	**Band**	**Spatial resol. (m)**	**Wavelength (μm)**	**Band**	**Spatial resol. (m)**	**Wavelength (μm)**
B 1-Blue	30	0.45–0.52	B 1-Blue	30	0.45–0.52	B 1- Ultra Blue	30	0.43–0.45
B 2-Green	30	0.52–0.60	B 2-Green	30	0.53–0.61	B 2-Blue	30	0.45–0.51
B 3-Red	30	0.63–0.69	B 3-Red	30	0.63–0.69	B 3-Green	30	0.53–0.59
B 4-NIR	30	0.76–0.90	B 4-NIR	30	0.78–0.90	B 4-Red	30	0.64–0.67
B 5-SWIR 1	30	1.55–1.75	B 5-SWIR 1	30	1.55–1.75	B 5-NIR	30	0.85–0.88
B 6-Thermal	120 (30) [II]	10.40–12.50	B 6-Thermal	60 (30) [III]	10.40–12.50	B 6- SWIR 1	30	1.57–1.65
B 7-SWIR 2	30	2.08–2.35	B 7-SWIR2	30	2.09–2.35	B 7- SWIR 2	30	2.11–2.29
–	–	–	B 8-Panchr.	30	0.52–0.90	B 8-Panchc.	15	0.50–0.68
–	–	–	–	–	–	B 9-Cirrus	30	1.36–1.38
–	–	–	–	–	–	B 10-TIR 1	100 (30) [IV]	10.60–11.19
–	–	–	–	–	–	B 11-TIR 2	100 (30) [IV]	11.50–12.51

Source: https://landsat.usgs.gov.
[II] TM Band 6 was acquired at 120-meter resolution, and was resampled to 30-meter pixels.
[III] ETM + Band 6 is acquired at 60-meter resolution, and was resampled to 30-meter pixels.
[IV] TIRS bands are acquired at 100 m resolution, and was resampled to 30 m in the delivered data product.

based on ground check-points of the Greater Cairo (Campbell & Wynne, 2011). The overall accuracy and kappa coefficient of the classified images were calculated by comparing classified data with 900 reference points for each studied date. The accuracy assessment (Table S2) exceeds recommendations by (Anderson, 1976; Thomlinson et al., 1999) that LULC mapping accuracy using Landsat imagery data should be Greater than 85 % and no single classified class<70 %.

2.3. Retrieval of land surface temperature (LST)

The standard method for retrieving LST from raw Landsat datasets requires the conversion of the digital numbers to radiance values of the thermal bands (Bands 10 and 11 in Landsat OLI/TIRS, and band 6 in Landsat 5 TM and Landsat 7 ETM +) first into absolute radiance values (Estoque et al., 2017). These bands pre-processed contain at-satellite brightness temperatures expressed in degrees Kelvin. To retrieve the LST, the at-satellite brightness temperature must be scaled using the emissivity of surface materials (ε) (Eq. (1)) (Sobrino et al., 2004), expressed as:

$$\varepsilon = m\,Pv + n \tag{1}$$

where $m = (\varepsilon_v - \varepsilon_s) - (1 - \varepsilon_s)\,F\varepsilon_v$ and $n = \varepsilon_s + (1 - \varepsilon_s)\,F\varepsilon_v$, where ε_v and ε_s are the vegetation emissivity and soil emissivity, respectively. The value of m (0.004) and n (0.986), according (Sobrino et al., 2004).

NDVI is the vegetation index derived using the surface reflectance of Landsat-8 Bands 4 (Red) and 5 (NIR), and surface reflectance of Landsat 5 and Landsat 7 Bands 3 (Red) and 4 (NIR) (Eq. (2)). According to Carlson & Ripley (1997), Pv represents the proportion of vegetation (Eq. (3)).

$$NDVI = \frac{(NIR - RED)}{(NIR + RED)} \tag{2}$$

$$Pv = \left(\frac{(NDVI - NDVImin)}{(NDVImax - NDVImin)}\right)^2 \tag{3}$$

The $NDVI_{max}$ and $NDVI_{min}$ are the maximum and minimum NDVI values, respectively.

Subsequently creating the images of emissivity, the emissivity-corrected values of LST were calculated as explained in Eq. (4) (Weng et al., 2004):

$$LST = TB/1 + \left(\frac{(\lambda \times TB)}{\rho}\right)\ln\varepsilon \quad (4)$$

Where λ is the wavelength of emitted radiance (λ = 10.8 μm, the centre wavelength of Landsat OLI/TIRS Band 10); TB is the Landsat OLI/TIRS Band 10 at-satellite brightness temperature (Estoque et al., 2017); ρ = h × c/σ (1.438 × 10–2 m K), σ = Boltzmann constant (1.38 × 10–23 J/K), h = Planck's constant (6.626 × 10^{-34} Js), and c = velocity of light (2.998 × 10^{8} m/s). In this study, we converted the retrieved LST values from Kelvin degrees into Celsius degrees (°C).

The future prediction of LST in 2030 was based on three steps, 1- converting the whole LST raster (30 m resolutions) of May, June, July and August over 1986, 2000, and 2017 to points shapefile, about 1.5 million points produced through this conversion; 2- applying linear regression prediction equation for the obtained

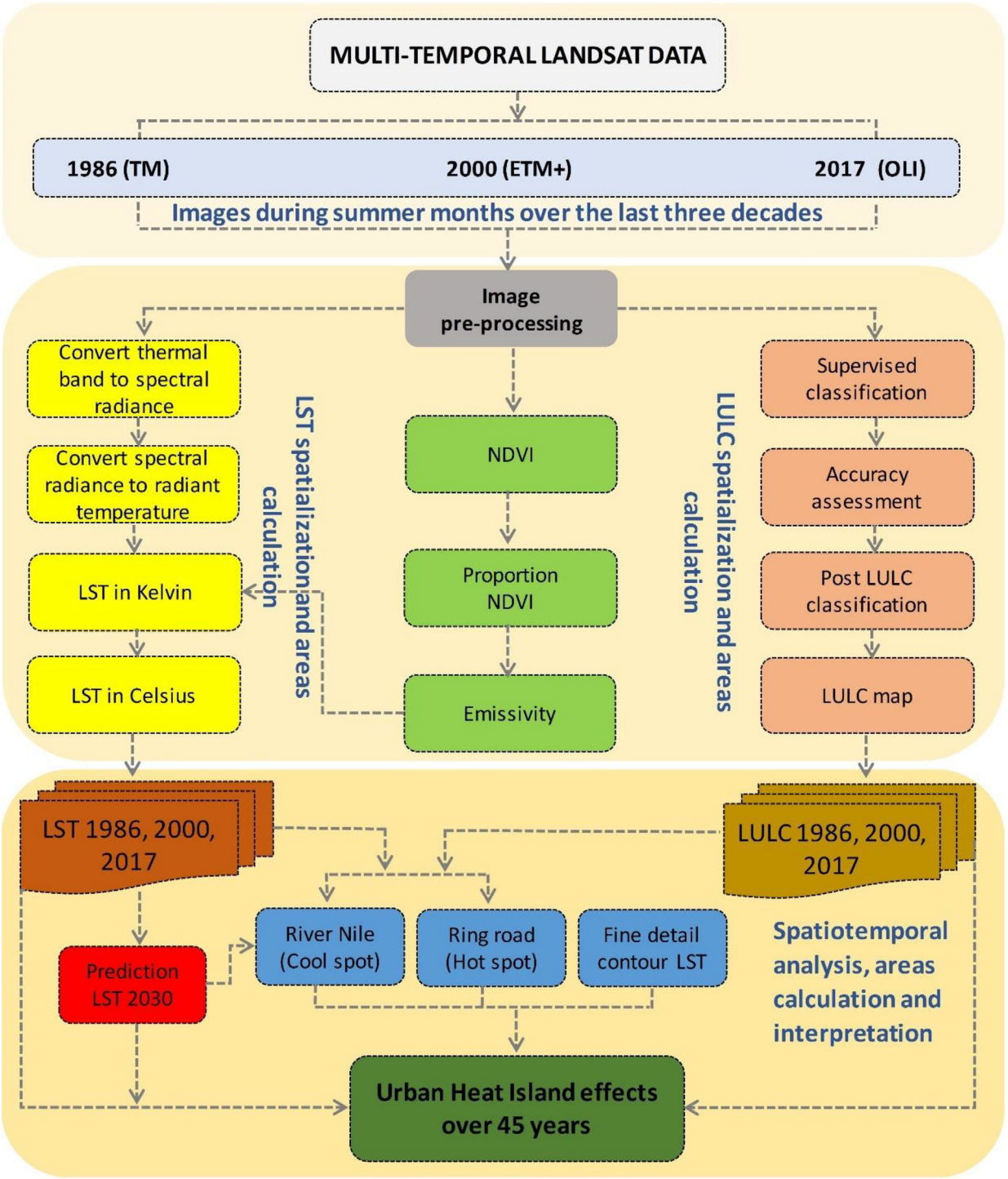

Fig. 2. Flowchart describing the overall methodology of land use / land cover (LULC) classification and land surface temperature (LST) retrieval.

points using Microsoft Excel FORECAST for 2030; 3- converting the predicted points shapefiles to raster conserving same resolutions (30 m) for summer months in 2030. In order to calculate LST values in summer months over 1986, 2000, 2017, and 2030 for dominant LULC (urban, urban associated with agriculture, agriculture associated with urban, agriculture, and water bodies), a focal analysis method was done for 330 plots (1 ha area) and to represent the LST variation of each LULC. Fig. 2 illustrates flowchart describing the overall methodology of land use / land cover (LULC) classification and land surface temperature (LST) retrieval.

3. Results

3.1. LULC in Greater Cairo

Greater Cairo is the most populated region in Egypt with a high population density (52,000/km^2). The population of Greater Cairo has doubled over the last three decades, where it was 11.2 million inhabitants in 1986, and became 22.8 million in 2017 and is expected to reach to 29 million by 2035. The dramatic increase of population has generated an inordinate change in LULC in the

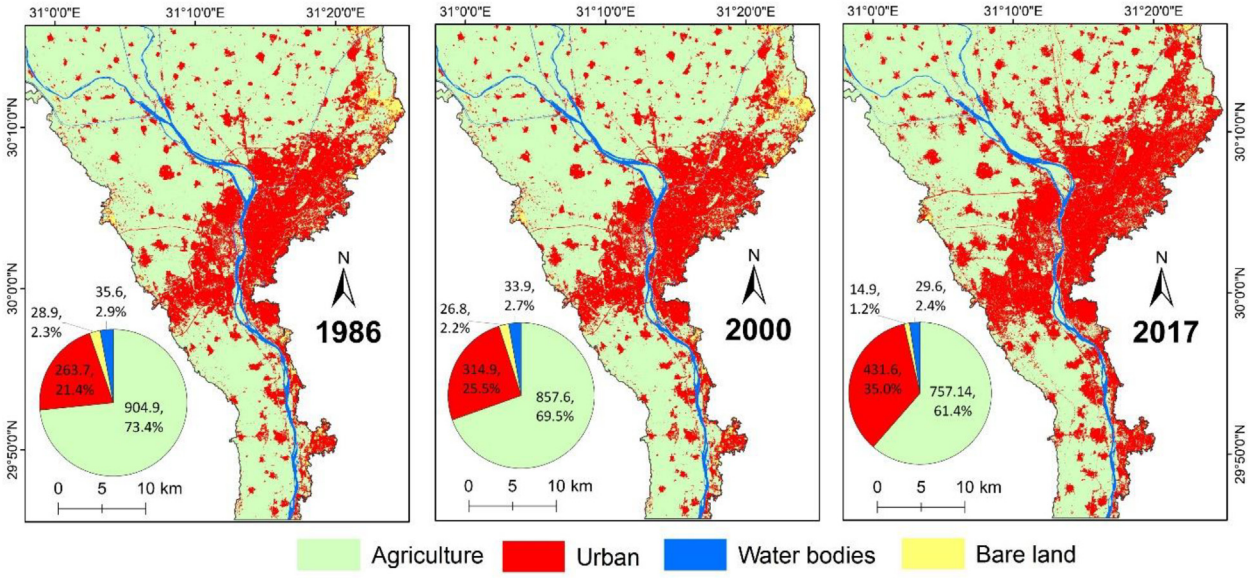

Fig. 3. LULC in Greater Cairo over a thirty-year period (1986, 2000, and 2017).

Fig. 4. Ground photos for the major LULC classes in grater Cairo. a) cultivated land; b) informal built-up areas; c) formal urban and roads; d) river Nile.

wider Greater Cairo area. TM and ETM+, and OLI Landsat images analysis reveals that the built-up areas including roads substantially increased over the last three decades. Built-up area increased from 21.4 % (263.7 km^2) in 1986 and reached 35.0 % (431.6 km^2) in 2017 (Fig. 3).

Much of the recent development has been in the form of unplanned informal built-up areas, which expanded rapidly and became more obvious after the 2011 Egyptian revolution. Recently the Egyptian government established new and restricted regulations to prevent urbanisation that draped over agricultural areas. Fig. 4 shows ground photos for the major LULC in Greater Cairo (i.e., cultivated land, informal built-up areas, formal urban, roads and river Nile). The results showed that the vegetated land was 73.4 % of the total area in 1986, decreasing by 3.9 % during 14 years to 2000, and a further decrease of 8.1 % from 2000 to 2017 (Fig. 3).

3.2. Spatio-Temporal changes of LST

Spatiotemporal analysis of LST was carried out for summer months (May to August) over 45 years (1986, 2000, 2017, and predicted for year 2030). Fig. 5 illustrates the increase in LST over the studied period where summer LST values were much lower in 1986 compared with 2000, 2017 and 2030. The increase in average LST during three decades was inversely proportional to the decrease in vegetative cover in the area during the period 1986 to 2017. Fig. 5 also shows that northern parts of the study area

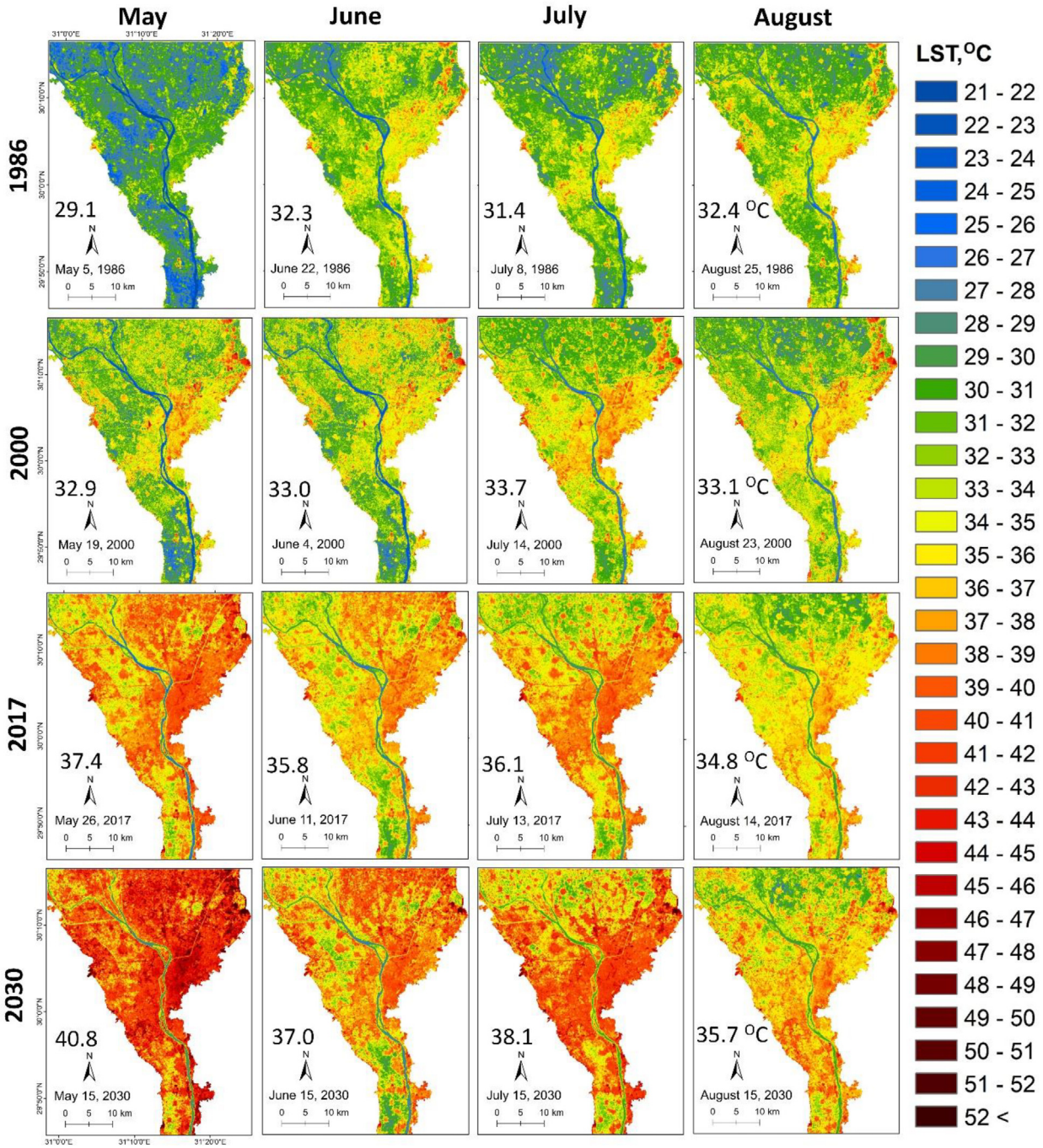

Fig. 5. Spatiotemporal analysis of land surface temperature for summer months (May, June, July and August) for three historical time points (1986, 2000, and 2017) and predicted year 2030.

have lower LST compared with the central parts. The timing of the hottest month varies over the time period. Some of the changes in LST between May and June may be due to agriculture practices linked to sowing dates and varying water requirements during the primary crop stage. The increment of mean LST in 2017 was high compared with 1986 and 2000 were the mean LST values was 37.4, 35.5, 36.1 and 34.8 °C and LST will getting hotter by 2030 were the mean LST will be 40.8, 37.0, 38.1, and 35.7 °C in May, June, July, and August, respectively. The increase of average LST over the last three decades was inversely proportional to the decrease in vegetative mass in the area during the period 1986–2017.

3.2.1. Changes of LST areas over 45 years

Within the whole studied area (1,234 km^2), the frequency distribution of LST (22–49 °C) was calculated for each summer month for three historical time points (1986, 2000, and 2017) and predicted year 2030 (Fig. 6). Temperatures have been steadily increasing, and the distribution of LST values affects the spatial patterns in Fig. 5. Overall, May shows the greatest increase in LST over time with a strong shift towards higher LST values. The other months show a shift in the modal part of the distribution while the lower and upper tails of the distribution do not shift as much.

3.3. LST classification

Fig. 7 illustrates the mean and variation in LST values over summer months for the dominant land cover types in greater Cairo during the last three decades (1986, 2000, and 2017) and 2030 predicted year. Estimates are based on a randomly selected set of 330 small plots (1 ha area) which have not changed in their classification for the duration. Urban land use has the highest LST values while water bodies have the lowest LST values. LST has consistently increased across all land cover types over the four time points, even for water and for agricultural land. The mean LST (1986–2017) of a suite of LULC has the following order: urban (34.3–38.8 °C) > urban associated with agriculture (33.5–37.5 °C) > agriculture associated with urban (31.0–35.3 °C) > agriculture (29.8–33.0 °C) > water bodies (24.5–27.8 °C).

The means of LST in Celsius over summer months in 1986 were 30.0 (May), 33.1(June), 32.5(July), and 33.6 (August), and increases were occurred during 2000 summer were 33.8 (May), 33.8 (June), 34.8(July), and 34.0 (August). In the same context, a considerable increase was observed in 2017 due to the unplanned urbanization, where the means of LST 37.6 (May), 36.0 (June), 36.7(July), and August (35.1). Consequently, the LST values have been increased over the studied thirty years by 7.6, 2.9, 3.2, 1.5 °C in May, June, July, and August respectively (Fig. 7). On the other hand, the predicted year 2030 showed that mean LST for whole area will increase by 2.7, 1.1, 1.8, and 0.7 °C for May, June, July, and August respectively compared with 2017. Table S3 illustrates the mean LST values for different LULC over the studied periods.

3.4. Fine detail contour maps of LST change over time

Six plots (each of 10 km^2) were selected over greater Cairo to illustrate fine scale variation in the pattern and change of LST over

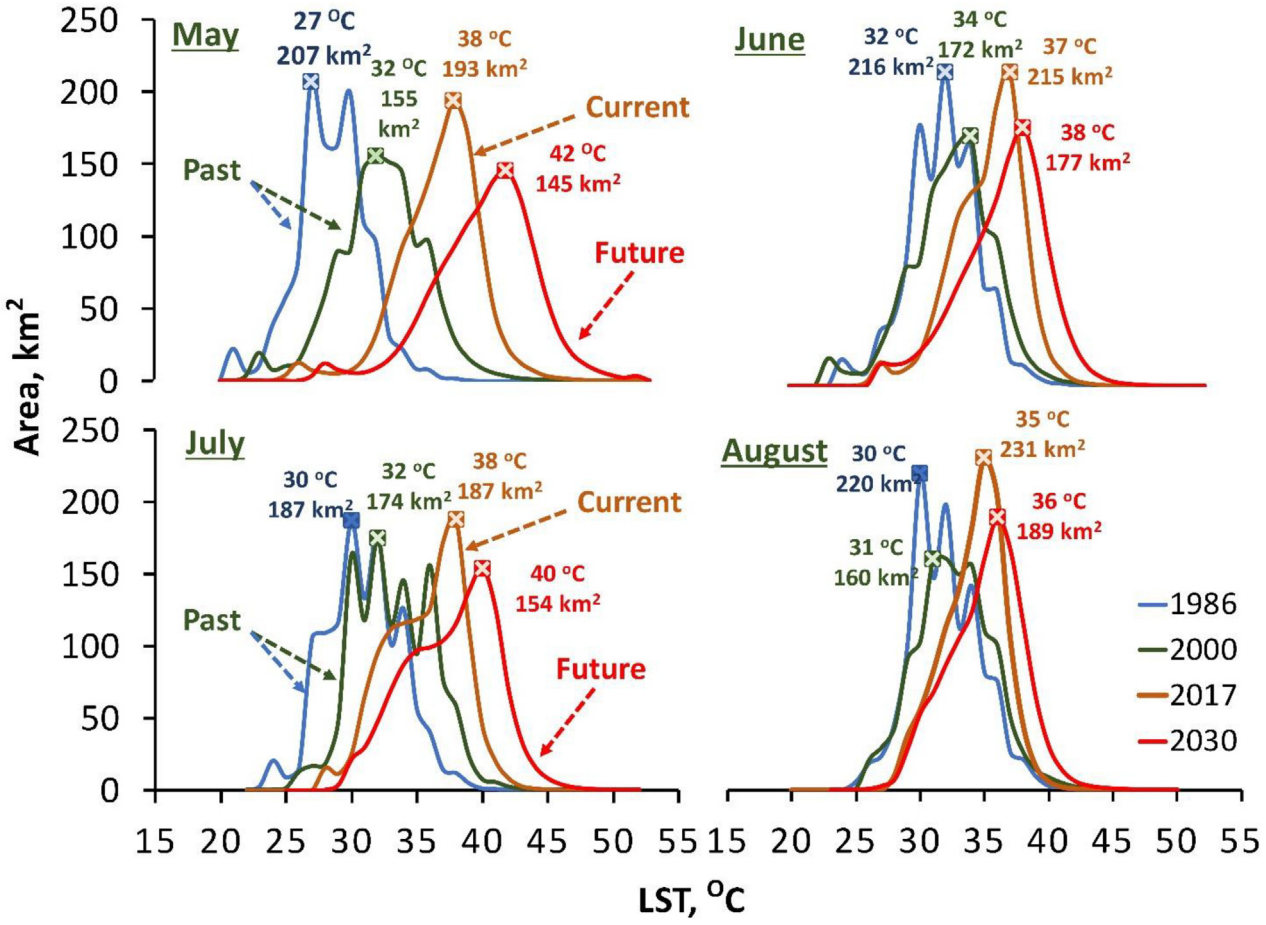

Fig. 6. Areas (km^2) of LST values (°C) during summer months over four decades (1986, 2000, 2017, and predicted year 2030) for Greater Cairo.

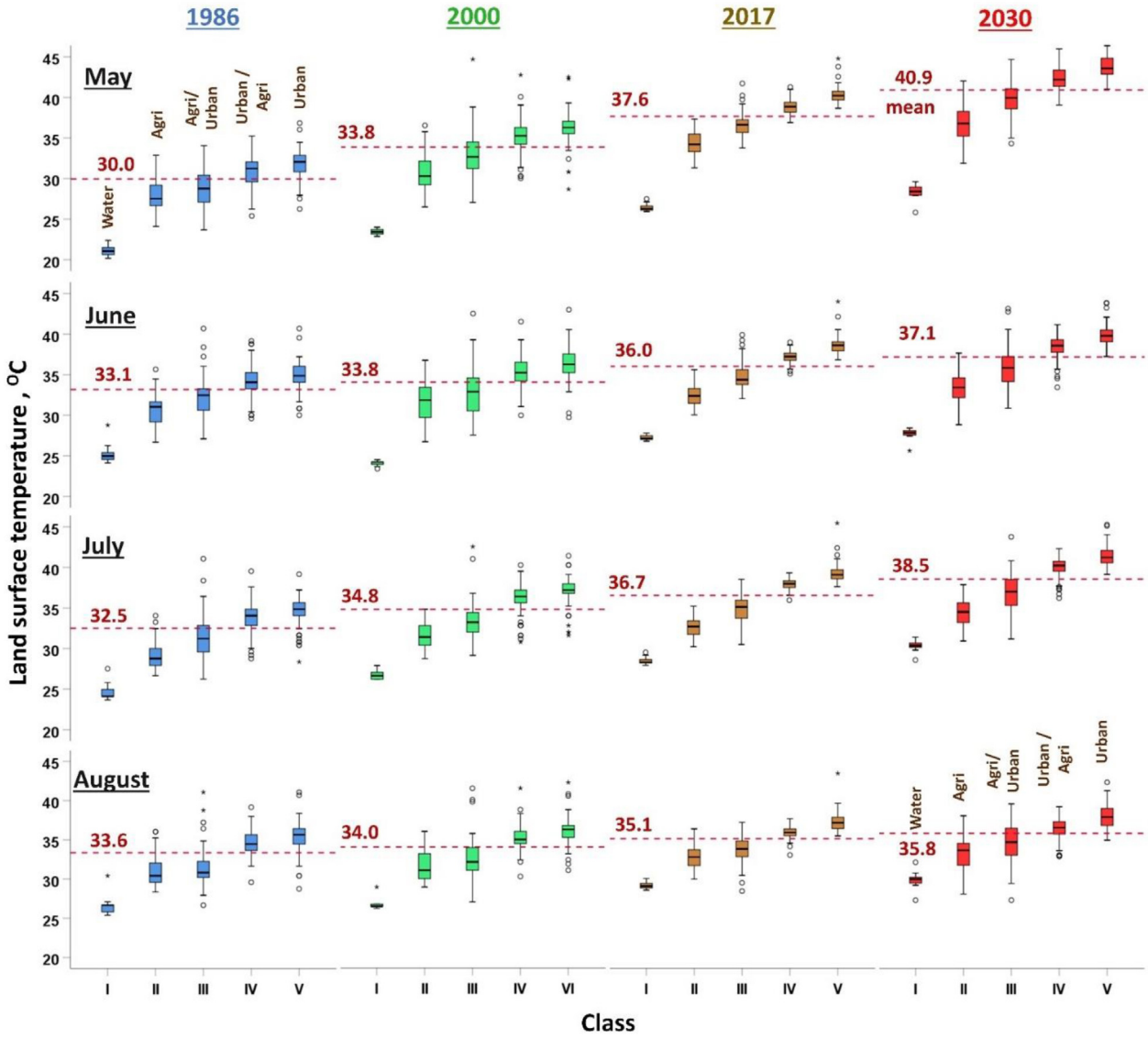

Fig. 7. Land surface temperature classification of the dominant LULC classes in summer months over 45 years (1986, 2000, 2017, and predicted year 2030) for Greater Cairo. LULC classes are I - Water, II - Agriculture, III - Majority agriculture with some urban, IV - Majority urban with some agriculture, V - Urban.

the last three decades (Fig. 8). The satellite images of each plot showing urban extent are illustrated in Fig. S1.

An increase of built-up areas and corresponding decrease in the surrounding agricultural land area leads to an increase in the LST over the last thirty years. Plot A is totally occupied by urban use and is located in the center of Cairo. This plot shows an increase of LST from 35.2 to 37.4 °C (2.2 °C) between 1986 and 2017. Plots D and E were located in the north of the study area and contain small patches of urban surrounded by agricultural land. These had the lowest LST over the studied period, but still show increases in LST. The influence of agricultural practices (e.g. irrigation of cultivated land) plays a role in reducing the LST (plot D). The south part of plot B was occupied by cultivated land in 1986, but was progressively replaced by urban areas up to 2017 leading to a 3.3 °C increase in LST. On the other hand, plots C and D demonstrated increases of urban areas with different extents that were surrounded by agriculture lands, and these enlargements led to an increase in the LST (Fig. 8). Plot F that is located in the south of the studied area and has higher LST compared with that of plot D (with which it shares a comparable proportion of urban extent).

3.5. Impacts of major roads (hot spots) and river Nile (cool spots) on LST

Large road systems directly increase the sealed area, and lead to an increase in associated urban development, which both increase LST. Meanwhile, water bodies act to cool LST. Here we explore the relative influence of these land cover types and how LST changes over time. The Egyptian government started establishing the ring road by 1986 and it was finished by 2005 with a total length of 100 km (El Araby, 2002). We evaluated urbanisation and UHI for the western part of the ring road with a length of 44 km and within a 2 km buffer zone to occupy a total area of 88 km^2. Within this zone, urban area has increased over the past thirty years from 21.3 km^2 in 1986 to 62.4 km^2 in 2017 replacing agricultural land (Fig. 9 a, b). On the other hand, the mean summer LST has increased from 31.1 °C in 1986 to 37 °C in 2017 (Fig. 9 c). The projected scenario of LST showed that the LST will increase by 1.9 °C in a period of 13 years (2017–2030). We assessed land use and LST change along the river Nile, and the adjacent 0.5 km buffer zone either side. Within this zone (Fig. 9 d), the total area of water

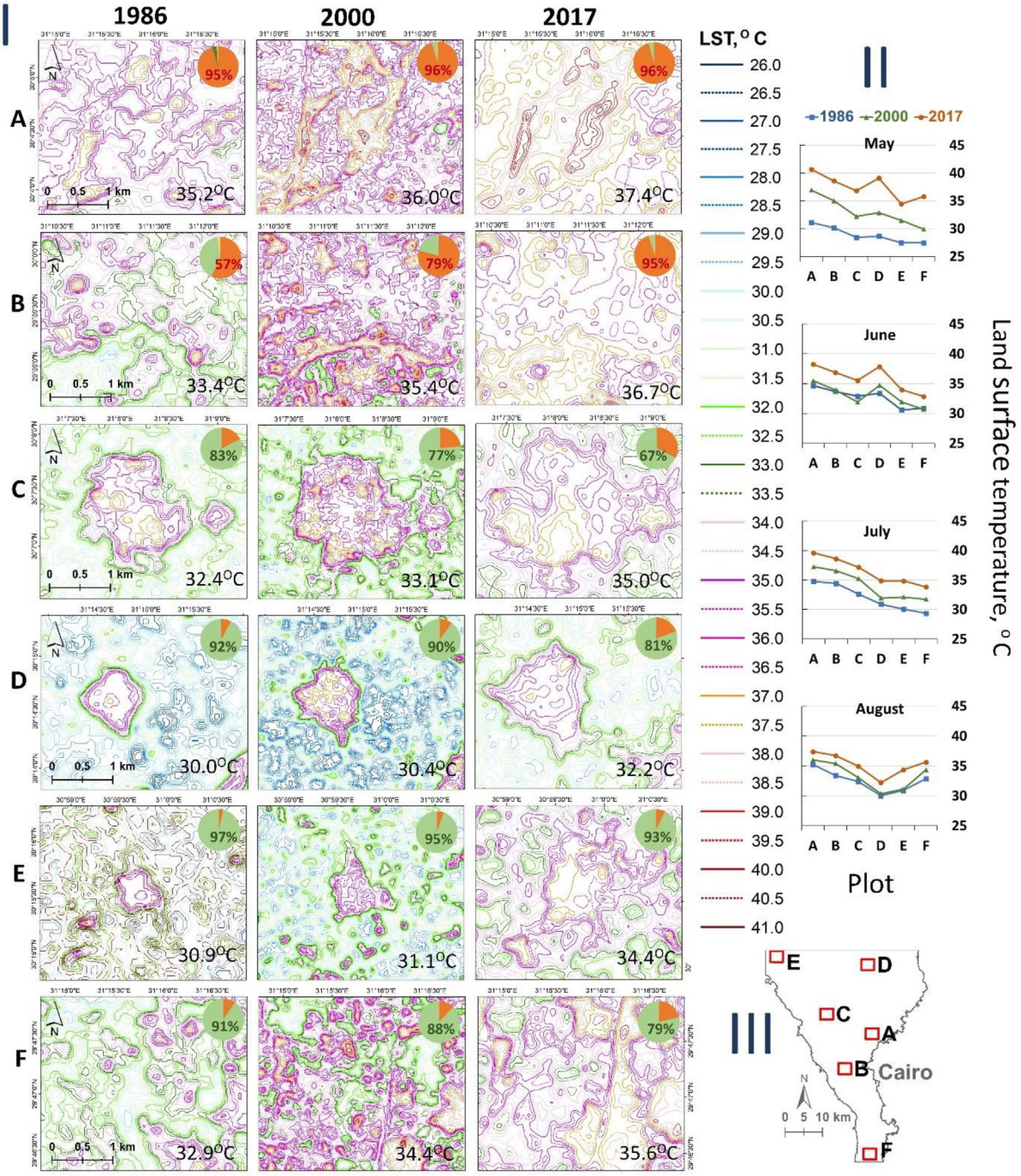

Fig. 8. Fine detail contour maps of land surface temperature, I) changes in the contour mean values of LST over the studied plots in August, II) LST mean by summer months for three historical time points (1986, 2000, and 2017) for the studied plots, III) location of plots within Greater Cairo. The small pie chart represents the percentages of urban (in orange) and cultivated land (in green). Plots A and B show the dominant LULC is urban, while plots B to F show agriculture coverage is the dominant LULC. (For interpretation of the references to colour in this figure legend, the reader is referred to the web version of this article.)

bodies was 35.6 km^2 (2.9 %) in 1986, decreasing to 33.9 km^2 (2.7 %) in 2000 and to 29.6 km^2 (2.4 %). This loss is primarily small isolated wetlands outside of the Nile itself, either directly to urbanisation or to agriculture. Although the total water body area is small it has a great impact on the LST, where the mean LST was much lower than for the ring road zone, showing 29.9 °C in 1986, and increasing to 34.2 °C in 2017 due to the rapid urbanisation in greater Cairo, and projected to reach to 35.9 °C in 2030 (Fig. 9e).

3.6. Overall changes in LST over 45 years

The mean summer LST of the whole greater Cairo area was 31.3 °C in 1986 and predicted to reach 37.9 °C in 2030, with an increase of 5.7 °C during the last 30 years (1986–2017) (Fig. 10a). When comparing agricultural areas with urban areas (and holding land area constant at 2017 extents), the mean LST in permanent agriculture areas (757 km^2) has increased substantially over the

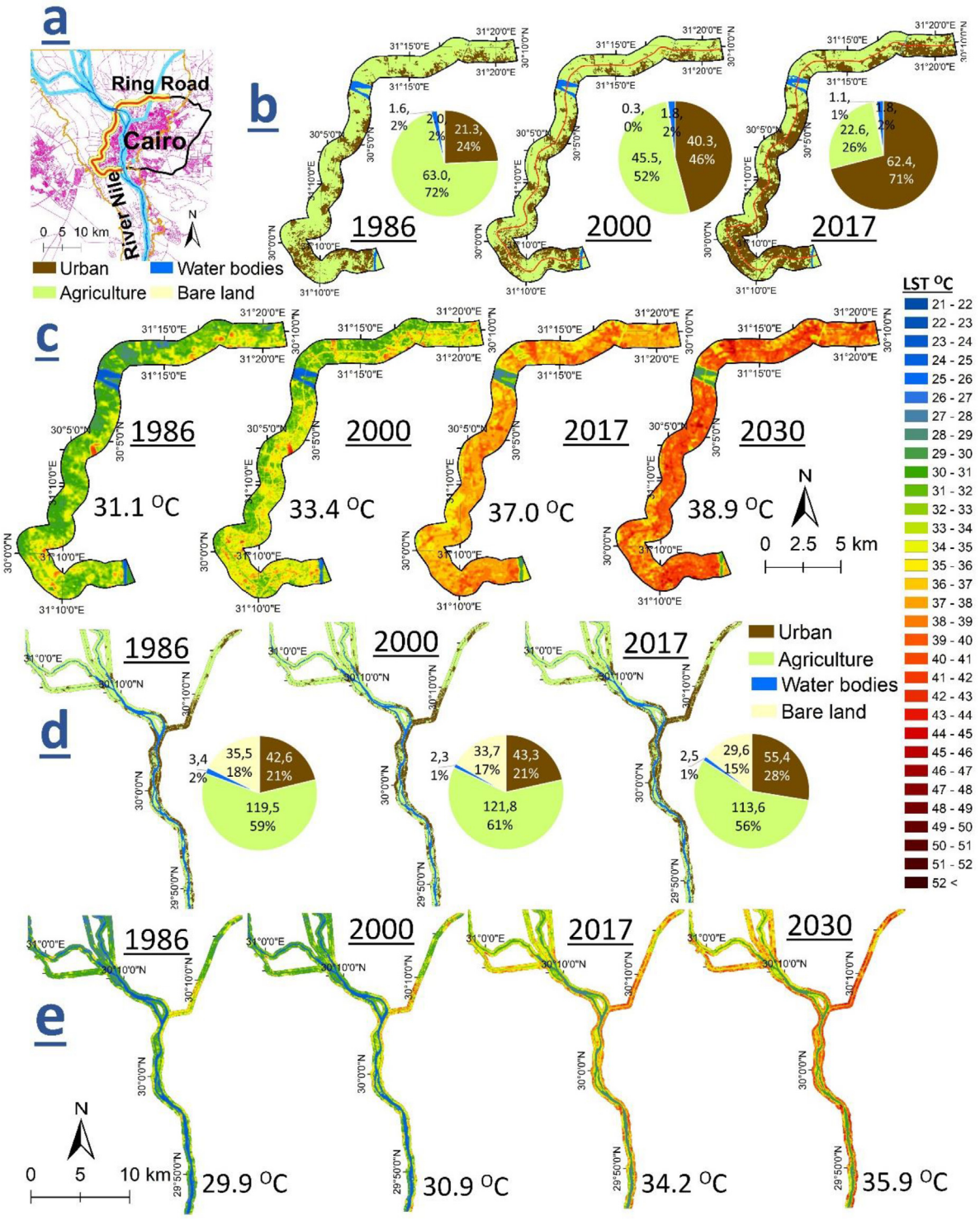

Fig. 9. Changes in LULC and land surface temperature along the western ring road, and the river Nile in Greater Cairo over the studied periods. Plots show: a) location of Ring Road, completed in 2005 and river Nile, b) LULC and proportion urban for the western ring road, at each time point 1986–2017, c) LST of western ring road for three time periods and projection to 2030 d) LULC around the river Nile, at each time point 1986–2017, e) LST of the river Nile for three time periods and projection to 2030.

three time periods, from 30.5 °C in 1986 to 35.0 °C in 2017 and is expected to reach 36.8 °C by the projected year 2030 (Fig. 10b).

For urban areas of 1986 (264 km^2), the mean LST has increased substantially over the three time periods, from 33.8 °C in 1986 to 38.1 °C in 2017 and it is expected to reach 39.9 °C by the projected year 2030 (Fig. 10C). The size of agriculture areas with mean LST greater than a 35 °C threshold for agricultural impacts was only 13 km^2 (0.02 %) in 1986 but increased to 31 km^2 (0.04 %, in 2000) with a huge increase to 350 km^2 (46 %) in 2017 and is predicted to reach 630 km^2 (83 %) of the total agriculture land by 2030. Moreover, the urban areas with a mean LST exceeding a 37 °C threshold for human thermal comfort increased from 9 km^2 (in 1986) to 349 km^2 (80 % in 2017) and is predicted to reach 414 km^2 (95 %) of total urban areas by 2030 (Fig. S2).

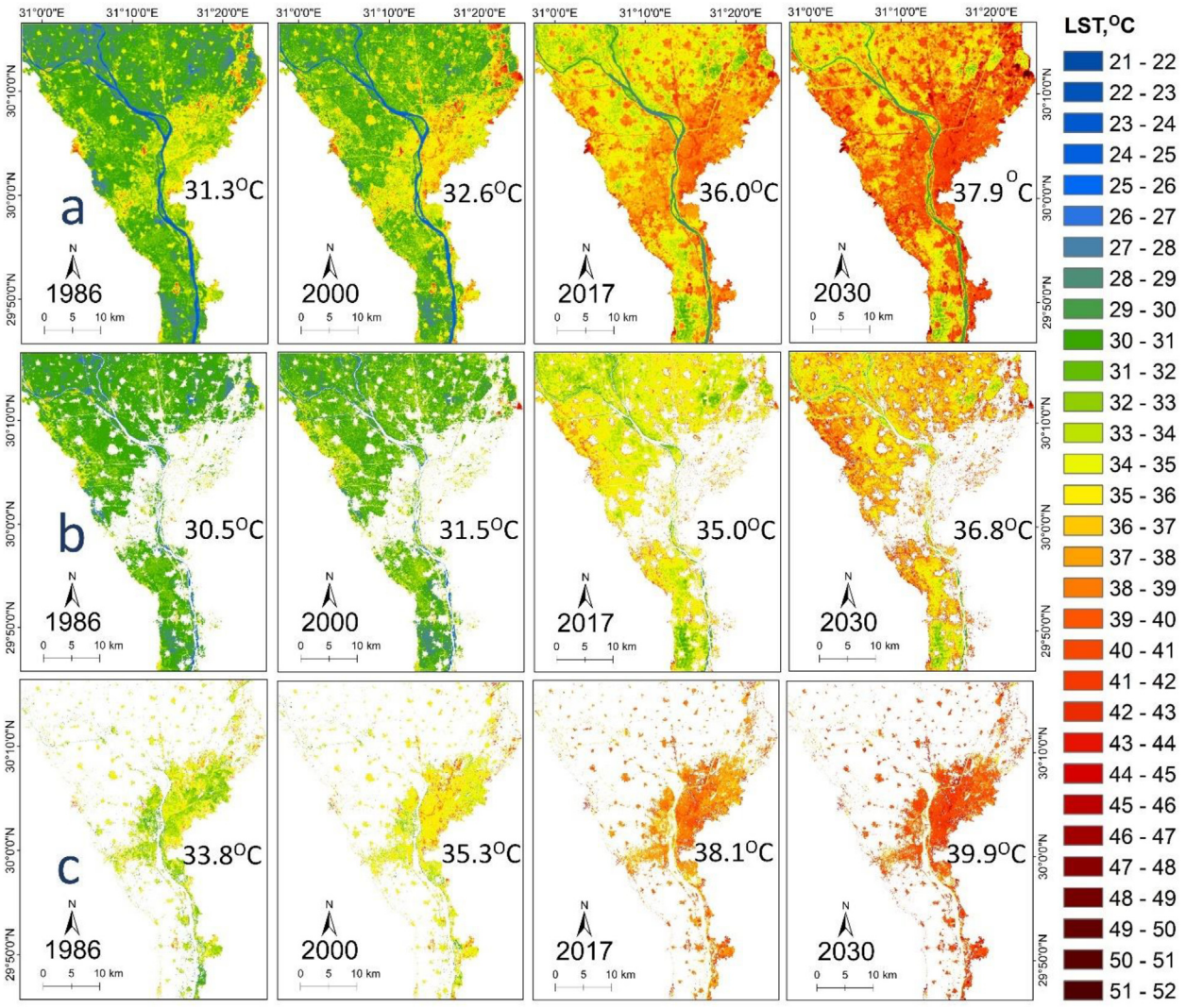

Fig. 10. Mean LST of summer months for whole greater Cairo (a), changes of LST in agricultural areas for three time periods and projection to 2030 (b), and changes of LST in urban areas for three time periods and projection to 2030. Extents of agricultural from 2017 and urban area from 1986 data only, to allow comparison of change in LST over time.

4. Discussion

This paper shows substantial increases in the extent of urban area in Greater Cairo, and the subsequent increases in LST, from 1986 to 2017, with additional projections to 2030, spanning 45 years in total. July temperature increases in urban areas and agricultural areas are broadly comparable over this time frame (4–7 °C increase), but when comparing hot spot areas around new development (Cairo ring road) and cool spot areas (the river Nile), temperatures appear to be rising faster in hot spots than in cool spots.

In this study, the rapid urban expansion in Greater Cairo is consistent with the general pattern of urban expansion in Egypt (Hendawy et al., 2019). It is also a prevalent pattern in the Middle East, and many countries around the world (Li et al., 2018; Ranagalage et al., 2020). The relationships between mean LST, urban and green density in some African cities have similar spatial patterns (Simwanda et al., 2019). Urbanisation may cause several socio-environmental problems, including enhanced sensitivity to climate change (Qiu et al., 2020), loss of fertile agriculture land (Abd-Elmabod et al., 2019) water and air contamination (Hereher et al., 2020), and environmental health (Grimm et al., 2008). These effects are particularly severe in large urban areas that have quickly urbanized without proper planning, and in arid and semi-arid regions (Abd-Elmabod et al., 2019).

UHI negatively affects agriculture (Mendez-Astudillo et al., 2022; Lin et al., 2022). In cultivated land, the increase in LST can affect crop phenological stage, pest resistance, leading to decreases in crop quality and yield (Kafy et al., 2021). Several crops are sensitive to increasing temperature, where each crop has an optimum temperature degree to achieve the maximum yield (Abd-Elmabod et al., 2020; Toulotte et al., 2022). Crops differ in their temperature tolerance thresholds (Marchin et al., 2022). Increasing LST also leads to an increase of evapotranspiration and consequently increases the irrigation water required for crops (Gaznayee et al., 2022). UHI also leads to negative impacts on the economy, while energy use will increase in wealthier areas through increased use of air conditioners. However, air conditioning systems also lead to an increase of both humidity and temperature outside of buildings, causing adverse impacts to the thermal comfort index of outdoor spaces in cities. The changes of regional climate due to UHI and the decline of cultivated land with its cooling potential may directly affect the soil organic carbon balance, irrigation water quality and may cause a range of environmental hazards,

especially in arid and semi-arid regions which are more susceptible to vegetation degradation (Abd-Elmabod et al., 2019; Abdel-Fattah et al., 2020; Jiménez-González et al., 2022).

In developing countries a linear relationship has been observed between road expansion and increasing land surface temperature (Aboelnour & Engel, 2018; Arulbalaji et al., 2020). Small isolated urban areas and roads represent micro UHI within cities or sub rural areas, and the intensity of UHI is dependent on land cover changes in the relative composition of vegetated land, water bodies, and built-up (Chen et al., 2006). Establishing road networks (in cities and villages) over cultivated land may have negative environmental impacts such as increasing LST, environmental pollution, increasing emission of greenhouse gases and air pollutants (Lu et al., 2018; Tsanova et al., 2021). These negative impacts have been observed in various countries in Europe, Asia, and Africa, and with particularly severe impacts noted in densely populated countries such as India and Egypt (Abdel Wahed & Abd El Monem, 2020; Kotharkar et al., 2018;). In the same context, isolated urban areas and roads represent micro UHI within cities or sub rural areas, and the intensity of UHI based on LULC change (Chen et al., 2006).

Cultivated land, green spaces, and water bodies are considered as the main cooling surfaces to mitigate the impacts of UHI and to help adapt to climate change (Du et al., 2017). In the surrounding atmosphere of cultivated lands and green spaces, increasing vegetation cover and water bodies or declining impervious surfaces will improve the benefits from green space cool island effects (Du et al., 2017). Cârlan et al. (2020) discuss that vegetative cover has different effects on UHI inside European cities, where the authors indicated that Bucharest in Romania showed a greater impact of vegetation cover on the magnitude of the UHI than Leipzig in Germany. Moreover, the density of roads and traffic inside both cities had a greater impact on LST than suburbs.

One important contributor to cooling in cities is water. In Greater Cairo water bodies decreased during the period from 1986 to 2017, and are likely to be further decreased due to continued urbanisation and the government's tendency to cover the canals inside Greater Cairo (Attia, 1999; Abd-Elmabod et al., 2019). Hence, the lack of water bodies and green spaces within Greater Cairo is likely to have contributed to the increasing LST during the last decade. Urban green and blue spaces mitigate UHI effects, especially in desert areas (bare land) where particularly high LST occurs. Vegetation in green space produces shade and absorbs the radiation energy by photosynthesis and transpiration, thus cooling down the LST (Wong and Yu, 2005).

The future projections on LST by 2030 are based on extrapolating current trends. These trends assume that historical temperature increases will increase linearly, and the projections are based on 2017 levels of urbanization being held constant. Since temperature will start to increase at a greater rate compared to current day (IPCC, 2022), and conversion of agricultural land to urban will continue to increase, these projections are highly likely to be an underestimate of future LST. Therefore, in future, the impacts on human health and on agriculture will likely be greater than projected here. In the same context, Lee et al. (2017) reported that with expected land use change in Hanoi, average air average temperature in new and existing urban areas will increase by up to 1 and 0.6 °C, respectively. In addition, by 2030, the average air temperature increases in existing urban areas may be up to 2.1 °C, of which, the contribution of 0.6 and 1.5 °C is attributable to land use and climate change respectively.

5. Conclusion

The applied approaches in this paper demonstrate substantial increase in LST over Greater Cairo, Egypt. These increases are slightly greater in heavily urbanised areas compared with cooler areas such as agriculture and water bodies. Establishing roads into agricultural land may accelerate urbanization and subsequently amplify UHI effects. The UHI may cause climate change, evapotranspiration rates variation and changes in LULC. The substantial areas of informal settlement have contributed to a large increase in land surface temperature. The means LST (1986–2017) of the diverse LULC have the following LST order: urban (34.3–38.8 °C) > urban associated with agriculture (33.5–37.5 °C) > agriculture associated with urban (31.0–35.3 °C) > agriculture (29.8–33.0 °C) > water bodies (24.5–27.8 °C). The mean LST of the permanent agricultural land has increased substantially from 30.5 °C in 1986 to 35.0 °C in 2017 and is expected to reach 36.8 °C by the projected year 2030. While for the built-up areas, the mean LST has increased substantially over 45 year period, from 33.8 °C in 1986 to 38.1 °C in 2017 and it is expected to reach 39.9 °C by the projected year 2030.

These results can support urban planners to understand the cooling benefits that come from cultivated land around cities, and can support the design of cool green spaces within Greater Cairo to mitigate UHI effects. However, increasing green areas in arid-climates will require a high amount of irrigation water especially under these desert conditions. Therefore, urban sprawl into desert spaces and an associated desire to increase the area of green and blue spaces, represents a major challenge for Egypt, particularly under conditions of water scarcity (<550 m^3 per capita per year). Therefore, planned urban, gardens and parks and green belts are needed to reduce UHI over densely urban areas. Such studies can assist decision makers to achieve more sustainable urban planning and to alleviate UHI stress on the environment.

Declaration of Competing Interest

The authors declare that they have no known competing financial interests or personal relationships that could have appeared to influence the work reported in this paper.

Acknowledgment

This work was supported by Ministry of Higher Education of the Arab Republic of Egypt under grant PD230. We acknowledge National Research Centre (Egypt) for funding the project No. 12050505. Also, the authors would like to thank the Scientific and Technological Innovation Fund of Carbon Emissions Peak and Neutrality of Jiangsu Provincial Department of Science and Technology (BE2022304).

Appendix A. Supplementary data

Supplementary data to this article can be found online at https://doi.org/10.1016/j.ejrs.2022.10.001.

References

Abdel Wahed, A.M.M., Abd El Monem, N., 2020. Sustainable and green transportation for better quality of life case study Greater Cairo-Egypt. HBRC Journal 16 (1), 17–37.
Abdel-Fattah, M.K., Abd-Elmabod, S.K., Aldosari, A.A., Elrys, A.S., Mohamed, E.S., 2020. Multivariate analysis for assessing irrigation water quality: A case study of the Bahr Mouise Canal. Eastern Nile Delta. Water 12 (9), 2537.
Abd-Elmabod, S.K., Fitch, A.C., Zhang, Z., Ali, R.R., Jones, L., 2019. Rapid urbanisation threatens fertile agricultural land and soil carbon in the Nile delta. J. Environ. Manage. 252, 109668.
Abd-Elmabod, S.K., Muñoz-Rojas, M., Jordán, A., Anaya-Romero, M., Phillips, J.D., Jones, L., Zhang, Z., Pereira, P., Fleskens, L., van der Ploeg, M., de la Rosa, D., 2020. Climate change impacts on agricultural suitability and yield reduction in a Mediterranean region. Geoderma 374, 114453.
Aboelnour, M., Engel, B.A., 2018. Application of remote sensing techniques and geographic information systems to analyze land surface temperature in

response to land use/land cover change in Greater Cairo Region. Egypt. Journal of Geographic Information System 10 (1), 57–88.
Abutaleb, K., Ngie, A., Darwish, A., Ahmed, M., Arafat, S., Ahmed, F., 2015. Assessment of urban heat island using remotely sensed imagery over Greater Cairo. Egypt. Advances in Remote Sensing 04 (01), 35–47.
Ali, R.R., Shalaby, A., 2012. Response of topsoil features to the seasonal changes of land surface temperature in the arid environment. Int. J. Soil Sci. 7 (2), 39–50.
Alves, E., Anjos, M., Galvani, E., 2020. Surface urban heat island in middle city: Spatial and temporal characteristics. Urban Science 4 (4), 54.
Anderson, J.R., 1976. A land use and land cover classification system for use with remote sensor data, Vol. 964. US Government Printing Office.
Arulbalaji, P., Padmalal, D., Maya, K., 2020. Impact of urbanisation and land surface temperature changes in a coastal town in Kerala. India. Environmental Earth Sciences 79 (17), 1–18.
Athukorala, D., Murayama, Y., 2021. Urban heat island formation in Greater Cairo: Spatio-temporal analysis of daytime and nighttime land surface temperatures along the urban–rural gradient. Remote Sensing 13 (7), 1396.
Attia, F.A.R., 1999. Water and Development in Greater Cairo (Egypt). Revista CIDOB d'Afers Internacionals, 81–102.
Awais, M., Li, W., Hussain, S., Cheema, M.J.M., Li, W., Song, R., Liu, C., 2022. Comparative evaluation of land surface temperature images from unmanned aerial vehicle and satellite observation for agricultural areas using in situ data. Agriculture 12 (2), 184.
J.B. Campbell R.H. Wynne Introduction to remote sensing (5th ed.). 2011 New York; London: Guilford.
Cârlan, I., Haase, D., Große-Stoltenberg, A., Sandric, I., 2020. Mapping heat and traffic stress of urban park vegetation based on satellite imagery-A comparison of Bucharest, Romania and Leipzig. Germany. Urban Ecosystems 23 (2), 363–377.
Carlson, T.N., Ripley, D.A., 1997. On the relation between NDVI, fractional vegetation cover, and leaf area index. Remote Sens. Environ. 62 (3), 241–252.
Chen, C., Bagan, H., Yoshida, T., Borjigin, H., Gao, J., 2022a. Quantitative analysis of the building-level relationship between building form and land surface temperature using airborne LiDAR and thermal infrared data. Urban Clim. 45, 101248.
Chen, H., Huang, J.J., Dash, S.S., McBean, E., Wei, Y., Li, H., 2022b. Assessing the impact of urbanisation on urban evapotranspiration and its components using a novel four-source energy balance model. Agric. For. Meteorol. 316, 108853.
Chen, X.-L., Zhao, H.-M., Li, P.-X., Yin, Z.-Y., 2006. Remote sensing image-based analysis of the relationship between urban heat island and land use/cover changes. Remote Sens. Environ. 104 (2), 133–146.
Chudnovsky, A., Ben-Dor, E., Saaroni, H., 2004. Diurnal thermal behavior of selected urban objects using remote sensing measurements. Energy Build. 36 (11), 1063–1074.
Du, H., Song, X., Jiang, H., Kan, Z., Wang, Z., Cai, Y., 2016. Research on the cooling island effects of water body: A case study of Shanghai, China. Ecol. Ind. 67, 31–38.
Du, H., Cai, W., Xu, Y., Wang, Z., Wang, Y., Cai, Y., 2017. Quantifying the cool island effects of urban green spaces using remote sensing Data. Urban For. Urban Greening 27, 24–31.
Duan, S.B., Li, Z.L., Zhao, W., Wu, P., Huang, C., Han, X.J., Shang, G., 2021. Validation of Landsat land surface temperature product in the conterminous United States using in situ measurements from SURFRAD, ARM, and NDBC sites. International Journal of Digital Earth 14 (5), 640–660.
Duveiller, G., Hooker, J., Cescatti, A., 2018. The mark of vegetation change on Earth's surface energy balance. Nat. Commun. 9 (1), 1–12.
El Araby, M., 2002. Urban growth and environmental degradation: The case of Cairo. Egypt. Cities 19 (6), 389–400.
Estoque, R.C., Murayama, Y., Myint, S.W., 2017. Effects of landscape composition and pattern on land surface temperature: An urban heat island study in the megacities of Southeast Asia. Sci. Total Environ. 577, 349–359.
Forstall, R. L., Greene, R. P., & Pick, J. B. (2004). Which are the largest? Why published populations for major world urban areas vary so greatly. City Futures Conference, University of Illinois at Chicago, Chicago, IL,
Gao, J., Gong, J., Yang, J., Li, J., Li, S., 2022. Measuring Spatial Connectivity between patches of the heat source and sink (SCSS): A new index to quantify the heterogeneity impacts of landscape patterns on land surface temperature. Landscape Urban Plann. 217, 104260.
Gaznayee, H.A.A., Al-Quraishi, A.M.F., Mahdi, K., Ritsema, C., 2022. A Geospatial Approach for Analysis of Drought Impacts on Vegetation Cover and Land Surface Temperature in the Kurdistan Region of Iraq. Water 14 (6), 927.
Goussous, J., Tayoun, L., 2020. A holistic approach to slum reduction: finding gaps in Cairo's 'how-to-deal'model with international collected experience. Cities & Health, 1–15.
Göttsche, F., Olesen, F., Trigo, I.F., Bork-Unkelbach, A., 2013. Validation of land surface temperature products with 5 years of permanent in-situ measurements in 4 different climate regions. In: In Proceedings of the EUMETSAT Meteorological Satellite Conference, Vienna, Austria, pp. 16–20.
Grimm, N.B., Faeth, S.H., Golubiewski, N.E., Redman, C.L., Wu, J., Bai, X., Briggs, J.M., 2008. Global change and the ecology of cities. Science 319 (5864), 756–760.
Hendawy, E., Belal, A., Mohamed, E., Elfadaly, A., Murgante, B., Aldosari, A.A., Lasaponara, R., 2019. The prediction and assessment of the impacts of soil sealing on agricultural land in the North Nile Delta (Egypt) using satellite data and GIS modeling. Sustainability 11 (17), 4662.
Hereher, M.E., Al-Awadhi, T., Mansour, S.A., 2020. Assessment of the optimized sanitary landfill sites in Muscat, Oman. The Egyptian Journal of Remote Sensing and Space Science 23 (3), 355–362.
X. Huang L. Hao G. Sun Z.L. Yang W. Li D. Chen Urbanisation aggravates effects of global warming on local atmospheric drying Geophysical Research Letters 49 2 2022 e2021GL095709.
Huang, H., Xue, Y., Chilukoti, N., Liu, Y., Chen, G., Diallo, I., 2020. Assessing global and regional effects of reconstructed land-use and land-cover change on climate since 1950 using a coupled land–atmosphere–ocean model. J. Clim. 33 (20), 8997–9013.
Ipcc, 2022. Climate Change 2022: Impacts, Adaptation, and Vulnerability. Contribution of Working Group II to the Sixth Assessment Report of the Intergovernmental Panel on Climate. Change Cambridge University Press.
Jiménez-González, M.A., Álvarez, A.M., Carral, P., Abd-Elmabod, S.K., Almendros, G., 2022. The pyrolytical fingerprint of nitrogen compounds reflects the content and quality of soil organic carbon. Geoderma, 116187.
Jin, M.S., Kessomkiat, W., Pereira, G., 2011. Satellite-observed urbanisation characters in Shanghai, China: Aerosols, urban heat island effect, and land–atmosphere interactions. Remote Sensing 3 (1), 83–99.
Kafy, A.-A., Rahman, A.F., Al Rakib, A., Akter, K.S., Raikwar, V., Jahir, D.M.A., Ferdousi, J., Kona, M.A., 2021. Assessment and prediction of seasonal land surface temperature change using multi-temporal Landsat images and their impacts on agricultural yields in Rajshahi. Bangladesh. Environmental Challenges 4, 100147.
Kotharkar, R., Ramesh, A., Bagade, A., 2018. Urban Heat Island studies in South Asia: A critical review. Urban Clim. 24, 1011–1026.
Lee, H.S., Trihamdani, A.R., Kubota, T., Iizuka, S., Phuong, T.T.T., 2017. Impacts of land use changes from the Hanoi Master Plan 2030 on urban heat islands: Part 2. Influence of global warming. Sustainable Cities and Society 31, 95–108.
Li, X., Yang, L., Ren, Y., Li, H., Wang, Z., 2018. Impacts of urban sprawl on soil resources in the Changchun-Jilin Economic Zone, China, 2000–2015. Int. J. Environ. Res. Public Health 15 (6), 1186.
Lin, M., Lin, T., Jones, L., Liu, X., Xing, L., Sui, J., Zhang, J., Ye, H., Liu, Y., Zhang, G., Lu, X., 2021. Quantitatively assessing ecological stress of urbanization on natural ecosystems by using a landscape-adjacency index. Remote Sensing 13 (7), 1352.
Lin, L.u., Meng, L., Mei, Y., Zhang, W., Liu, H., Xiang, W., 2022. Spatial–temporal patterns of summer urban islands and their economic implications in Beijing. Environ. Sci. Pollut. Res. 29 (22), 33361–33371.
Lu, M., Taiebat, M., Xu, M., Hsu, S.-C., 2018. Multiagent spatial simulation of autonomous taxis for urban commute: Travel economics and environmental impacts. J. Urban Plann. Dev. 144 (4), 04018033.
Marchin, R.M., Backes, D., Ossola, A., Leishman, M.R., Tjoelker, M.G., Ellsworth, D.S., 2022. Extreme heat increases stomatal conductance and drought-induced mortality risk in vulnerable plant species. Glob. Change Biol. 28 (3), 1133–1146.
McNabb, D.E., 2019. The population growth barrier. In Global pathways to water sustainability. In: McNabb, D.E. (Ed.), Global Pathways to Water Sustainability. Springer International Publishing, Cham, pp. 67–81.
Mendez-Astudillo, J., Lau, L., Tang, Y.T., Moore, T., 2022. Determination of Air Urban Heat Island Parameters with High-Precision GPS Data. Atmosphere 13 (3), 417.
Miao, S., Zhan, W., Lai, J., Li, L., Du, H., Wang, C., Wang, C., Li, J., Huang, F., Liu, Z., Dong, P., 2022. Heat wave-induced augmentation of surface urban heat islands strongly regulated by rural background. Sustainable Cities and Society 82, 103874.
Qiu, T., Song, C., Zhang, Y., Liu, H., Vose, J.M., 2020. Urbanization and climate change jointly shift land surface phenology in the northern mid-latitude large cities. Remote Sens. Environ. 236, 111477.
Ranagalage, M., Ratnayake, S.S., Dissanayake, DMSLB, Kumar, L., Wickremasinghe, H., Vidanagama, J., Cho, H., Udagedara, S., Jha, K.K., Simwanda, M., Phiri, D., Perera, ENC, Muthunayake, P., 2020. Spatiotemporal variation of urban heat islands for implementing nature-based solutions: A case study of Kurunegala, Sri Lanka. ISPRS Int. J. Geo-Inf. 9 (7), 461.
Ritchie, H., & Roser, M. (2018). Urbanisation. Our world in data. Retrieved August, 7, 2020.
Simwanda, M., Ranagalage, M., Estoque, R.C., Murayama, Y., 2019. Spatial analysis of surface urban heat islands in four rapidly growing African cities. Remote Sensing 11 (14), 1645.
Sobrino, J.A., Jiménez-Muñoz, J.C., Paolini, L., 2004. Land surface temperature retrieval from LANDSAT TM 5. Remote Sens. Environ. 90 (4), 434–440.
Thomlinson, J.R., Bolstad, P.V., Cohen, W.B., 1999. Coordinating methodologies for scaling landcover classifications from site-specific to global: Steps toward validating global map products. Remote Sens. Environ. 70 (1), 16–28.
Toulotte, J.M., Pantazopoulou, C.K., Sanclemente, M.A., Voesenek, L.A., Sasidharan, R., 2022. Water stress resilient cereal crops: Lessons from wild relatives. J. Integr. Plant Biol. 64 (2), 412–430.
Tsanova, D., Vekov, T., Seizov, A., Statev, K., 2021. How do different sources contribute to population exposure to key air pollutants in Bulgaria. Trakia Journal of Sciences 19 (4), 303.
USGS (United States Geological Survey), 2016. Product Guide: Provisional Landsat 8 Surface Reflectance Product. Department of the Interior, U.S. Geological Survey.
Wang, Y., Zhang, Y., Sun, W., Zhu, L., 2022. The impact of new urbanisation and industrial structure changes on regional water stress based on water footprints. Sustainable Cities and Society 103686.

Weng, Q., Lu, D., Schubring, J., 2004. Estimation of land surface temperature–vegetation abundance relationship for urban heat island studies. Remote Sens. Environ. 89 (4), 467–483.
Wong, N.H., Yu, C., 2005. Study of green areas and urban heat island in a tropical city. Habitat international 29 (3), 547–558.
Xian, G., Shi, H., Zhou, Q., Auch, R., Gallo, K., Wu, Z., Kolian, M., 2022. Monitoring and characterizing multi-decadal variations of urban thermal condition using time-series thermal remote sensing and dynamic land cover data. Remote Sens. Environ. 269, 112803.
Yan, Y., Liu, T., Wang, N., Yao, S., 2022. Urban sprawl and fiscal stress: Evidence from urbanizing China. Cities 126, 103699.
Zhao, Y.-G., Zhang, G.-L., Zepp, H., Yang, J.-L., 2007. Establishing a spatial grouping base for surface soil properties along urban–rural gradient—A case study in Nanjing. China. Catena 69 (1), 74–81.
Zhou, D., Sun, S., Li, Y., Zhang, L., Huang, L., 2022. A multi-perspective study of atmospheric urban heat island effect in China based on national meteorological observations: Facts and uncertainties. Sci. Total Environ. 158638.